Hopf Bifurcation Control of Power Systems Nonlinear Dynamics Via a Dynamic State Feedback Controller–Part II: Performance Evaluation

Pouya Mahdavipour Vahdati, *Graduate Student Member, IEEE*, Luigi Vanfretti, *Senior Member, IEEE*, M. Hadi Amini, *Graduate Student Member, IEEE*, and Ahad Kazemi

***Abstract*—This is the second part of a two-part paper presenting a dynamic state feedback control law that guarantees the elimination of Hopf bifurcations before the occurrence of a saddle-node bifurcation (SNB). In Part I, the mathematical representation of the system's dynamics, Hopf and Saddle-Node bifurcation theorems, and the state feedback controller design were presented.**

In this part, to illustrate the system analysis methodology, control design, and to carry out performance evaluation of the controller, both single-machine and multi-machine power systems are analyzed. To highlight the effect of saturation phenomena, bifurcation analyses are performed before and after detailed modeling of synchronous generator saturation, for the single-machine power system case. The multi-machine case is used to illustrate the scalability and applicability of the method to generic power networks.

***Index Terms*—Bifurcation analysis, Hopf bifurcation, stable equilibrium point, saddle-node bifurcation, saturation phenomenon, stability analysis.**

I. Introduction

Voltage instability mechanisms have been widely studied in the literature [1]–[8], with detailed analyses on bifurcations in [9]. Based on these studies, it is concluded that collapse in the voltage profile of the system can occur before reaching the maximum loadability margin of the system, which is the saddle-node bifurcation. This is due to the occurrence of Hopf bifurcations in the stationary branch of solutions, which introduce oscillatory behavior in system responses that to system collapse [4], [5].

Catastrophic failures in the power system can cause destructive blackouts [10]. Moreover, the security challenges of future power systems play a pivotal role in power system stability [11]. In addition, studies have been made on the prevention of voltage collapse due to the phenomena described above [12]–[14]. Most of these studies make use of FACTS devices in order to eliminate Hopf bifurcations from system responses. The application of classical control methods have been investigated in [15]–[17], which are able to control only one Hopf bifurcation in system. In [18] - the first part of this paper - a dynamic state feedback control law has been introduced to guarantee the elimination of Hopf bifurcations before the occurrence of a saddle-node bifurcation (SNB). In other words, the proposed method helps to prevent the voltage collapse before reaching the SNB, by preserving the structural stability of the system.

This paper, illustrates and analyses the performance of the state feedback controller proposed in Part I [18] and the effectiveness of the controller in terms of instability prevention before the saddle-node bifurcation (SNB) is evaluated. The remainder of this paper is organized as follows,

Secion II describes the implementation of the analysis method in [18]. Sections III and IV perform bifurcation analyses on two power networks under study, while Section V illustrates the controller design and asses the performance of the controller. Finally, conclusions are drawn in Section VI.

II. Analysis Method Implementation

The analysis framework for the proposed nonlinear state feedback controller is provided in Fig. 1. To implement the proposed nonlinear state-feedback controller in Fig. 1 of [18], two prototype implementations were carried out as sketched in Figs. 2 and 3.

The first implementation, uses MATCONT [19] which is a generic nonlinear dynamical systems analysis software, and aims to illustrate the application of the proposed method using a 3-node power system. First, the equations of the dynamical model of the system are derived from equations (10)-(13) of [18], and the parameters and constants used herein are provided in the Appendix. Next, the ODE model of the system is implemented using MATCONT's syntax. The stable equilibrium of the system is derived by solving these equations while equating the derivatives to zero, and checking the eigenvalues of the Jacobian matrix for each derived equilibria. Solutions for equilibria are derived using the `fsolve` routine in MATLAB, and the stability of the equilibria through the eigenvalues of the Jacobian are checked through customized code. After the derivation of the SEP, the bifurcation analysis routine is initialized and executed

P. Mahdavipour Vahdati is supported by the EUs H2020 under grant agreement no 674875. Innovative Training Network oCPS.

L. Vanfretti was supported in part by the StandUP for Energy Collaboration Initiative and the ITEA3 project 14018 - OPENCPS.

P. Mahdavipour Vahdati and A. Kazemi are with Center of Excellence for Power Systems Automation and Operation, Iran University of Science and Technology, Tehran, Iran. P. M. Vahdati is also with Department of Machine Design, KTH Royal Institute of Technology, Stockholm, Sweden. M. H. Amini is with the Department of Electrical and Computer Engineering, Carnegie Mellon University, Pittsburgh, PA 15213, USA. He is also with SYSU-CMU Joint Institute of Engineering. L. Vanfretti is with Smart Transmission Systems Lab (SmarTS Lab), KTH Royal Institute of Technology, Stockholm, Sweden. e-mails: pouyamv@kth.se, kazemi@iust.ac.ir, amini@cmu.edu, luigi.vanfretti@ee.kth.se.

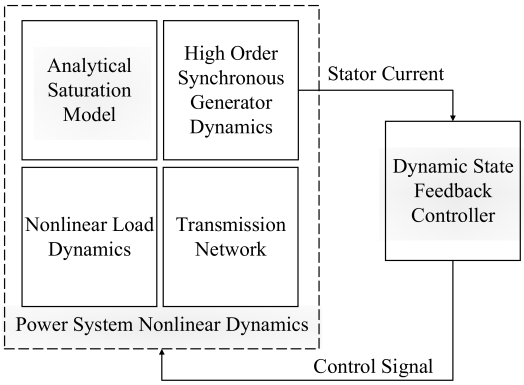

Fig. 1. General analysis framework of the proposed nonlinear state feedback controller for Hopf bifurcation control

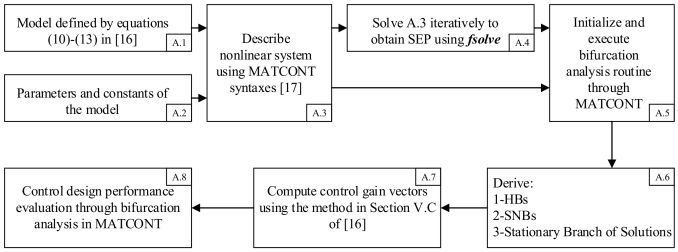

Fig. 2. Implementation of the method for the single-machine system analysis

in MATCONT. The results of the bifurcation analysis give the coordinates of the stationary branch of solutions, Hopf bifurcations and also the Saddle-Node bifurcation. Next, these results are used to compute the control gain vectors with the method described in Section V.C of [18]. After the calculation of control gain vectors, the controller is added to the dynamics of the system, and the bifurcation analysis is performed again to evaluate the performance of the controller in relocating the Hopf bifurcations from stationary branch of solutions. This implementation is depicted in Fig. 2.

Because the implementation in Fig. 2 was carried out in a generic nonlinear dynamical systems analysis software, it is difficult to scale the same implementation for multi-machine systems. Hence, the implementation in Fig. 3 is carried out using a power system specific tool, i.e. PSAT [20].

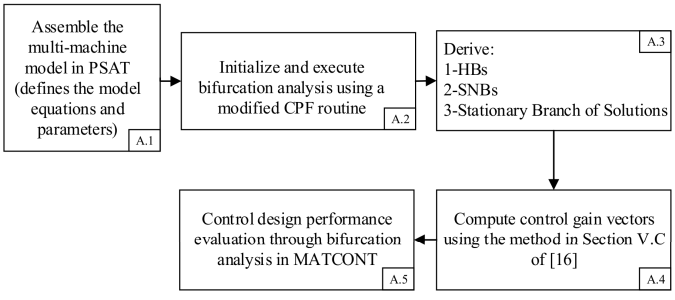

Fig. 3. Implementation of the method for the multi-machine system analysis

TABLE I
BIFURCATIONS OF THE SYSTEM W.R.T. ACTIVE LOAD NEGLECTING SATURATION

$Point\ Type$	EP	HB	SNB
P_{ld}	0	0.462177	0.942336

TABLE II
BIFURCATIONS OF THE SYSTEM W.R.T. ACTIVE LOAD CONSIDERING SATURATION

$Point\ Type$	EP	HB_1	HB_2	SNB
P_{ld}	0	0.623944	1.018561	1.024110

III. BIFURCATION ANALYSIS OF THE SINGLE-MACHINE TEST SYSTEM

In this section, bifurcation analysis on the single-machine nonlinear dynamic power system is performed. To investigate the effects of detailed saturation modeling, the system dynamics are analyzed with and without modeling of saturation effects. MATCONT, a MATLAB package for numerical bifurcation analysis of ODEs is used for performing the bifurcation analysis [19]. The bifurcation parameters of the system are the active and reactive power demands of the nonlinear load. Next, the controller is designed with appropriate gains to relocate Hopf bifurcations to equilibria located after the SNB.

A. Bifurcation Analysis w.r.t. P_{ld}

In this section, the nonlinear behavior of the uncontrolled system w.r.t. P_{ld} is investigated. Analysis has been performed with and without modeling saturation. The results of the analysis are provided in Tables I and II and Figs. 4 and 5.

First, the system without saturation modeling is investigated. The results of the bifurcation analysis are presented in Table I and Fig.4. In this case, the system undergoes only one Hopf bifurcation. Further increase in active power demand will cause system collapse. Let $\zeta_L^{(1)}$ denote the first Lyapunov coefficient of the Hopf bifurcation, it occurrs at $P_{ld} = 0.462177$ and is $\zeta_{L_{H1}}^{(1)} = -0.01389562$. Because $\zeta_{L_{H1}}^{(1)} < 0$, the resulting limit cycles are stable and the bifurcation is supercritical. Nevertheless, the fixed solutions of the system lose stability because a of pair of conjugate eigenvalues cross the imaginary axis, as shown in Fig.5.

The results of the bifurcation analysis when modeling saturation are presented in Table II. It is observed that the system undergoes two Hopf bifurcations and that any further increase in active power demand will lead the system to collapse. With the occurrence of Hopf bifurcations, limit cycles emerge. As it is observed, the stationary branch of solutions is stable until the first Hopf bifurcation occurs. The first Lyapunov coefficient of the first Hopf bifurcation occuring at $P_{ld} = 0.623944$ is $\zeta_{L_{H1}}^{(1)} = -0.01938673$. Because $\zeta_{L_{H1}}^{(1)} < 0$, the resulting limit cycles are stable and the bifurcation is supercritical. However, the system loses stability because of the pair of complex conjugate eigenvalues cross the imaginary axis, as shown in Fig.5.

For the second Hopf bifurcation occurring at $P_{ld} = 1.018561$ before the SNB, the first Lyapunov coefficient is

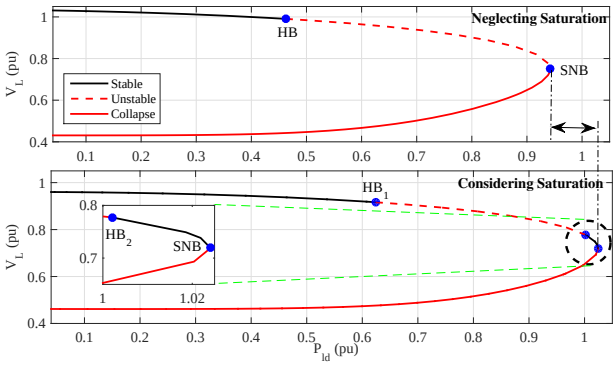

Fig. 4. Bifurcation analysis w.r.t. P_{ld} (Top: Neglecting Saturation. Bottom: Considering Saturation)

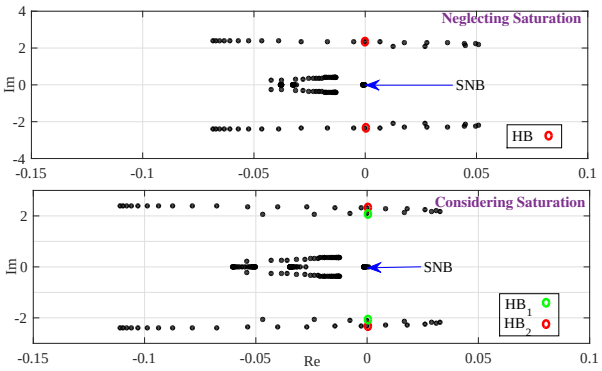

Fig. 5. Eigenvalues of the system after bifurcation analysis w.r.t. P_{ld} (Top: Neglecting Saturation. Bottom: Considering Saturation)

$\zeta^{(1)}_{L_{H2}} = -0.05600226$. Because $\zeta^{(1)}_{L_{H2}} < 0$, this bifurcation is also supercritical and the limit cycles that emerge from it are stable. When the second Hopf bifurcation is reached, the system re-gains stability in the stationary branch because the same pair of eigenvalues that crossed the imaginary axis due to the first Hopf bifurcation, cross the axis again and stabilize the system. In addition, it is observed that the eigenvalues cross the imaginary axis two times and hence two Hopf bifurcations occur. By further increasing the bifurcation parameter, it is observed that the SNB occurs at $P_{ld} = 1.024110$ and that the stationary branch of solutions loses structural stability. After this point, no stable operating point could be found for the system. The bifurcation diagrams and the eigenvalue loci of the system for both cases are illustrated in Figs. 4 and 5.

Detailed saturation modeling provides a richer representation of the nonlinear behavior of the system. As depicted in Fig. 4, when saturation is explicitly modeled in the dynamical equations of the system, two Hopf bifurcations occur. However, neglecting saturation leads to simpler dynamics, as one Hopf bifurcation is not represented. Further, results considering saturation show a $0.081774\ pu$ higher loadability margin for the system. In other words, the system does not collapse at $P_{ld} = 0.942336$, which is the active load demand for which SNB occurs when saturation is not modeled. Consequently, in addition to unrepresented bifurcations, the loadability margins obtained from bifurcation analysis without considering saturation are not accurate. Considering the saturation phenomenon effectively contributes to the accuracy of stability analyses and in devising voltage instability prevention measures.

B. Bifurcation Analysis w.r.t. Q_{ld}

In this section, the nonlinear behavior of the uncontrolled system w.r.t. Q_{ld} is investigated. analyses have been performed with and without modeling saturation effects. The results are provided in Tables III and IV and Figs. 6 and 7.

First, the system without saturation modeling is investigated. The results of the bifurcation analysis are presented in Table III. Bifurcation analysis results show no Hopf bifurcations in the system dynamics. The system collapses at $Q_{ld} = 0.514804$ which is the SNB point.

TABLE III
BIFURCATIONS OF THE SYSTEM W.R.T. REACTIVE LOAD NEGLECTING SATURATION

Point Type	EP	SNB
Q_{ld}	0	0.514804

The results of the bifurcation analysis w.r.t. Q_{ld} when saturation is modeled are shown in Table IV. In this case, the system undergoes one Hopf bifurcation. The stationary branch of solutions is stable until the Hopf bifurcation occurs. The first Lyapunov coefficient of the Hopf bifurcation occurring at $Q_{ld} = 0.717763$, is $\zeta^{(1)}_{L_{H1}} = 1.612584$. Hence the bifurcation is subcritical. By further increasing the bifurcation parameter, it is observed that the SNB occurs at $Q_{ld} = 0.720344$ and the stationary branch of solutions loses structural stability. After this point, no stable operating point could be found for the system. The subcritical Hopf bifurcation will lead to unstable limit cycles, which cause voltage instability before reaching the SNB. The bifurcation diagrams of the system for both cases are shown in Fig. 6. As depicted in Fig. 6,

TABLE IV
BIFURCATIONS OF THE SYSTEM W.R.T. REACTIVE LOAD CONSIDERING SATURATION

Point Type	EP	HB	SNB
P_{ld}	0	0.717763	0.720344

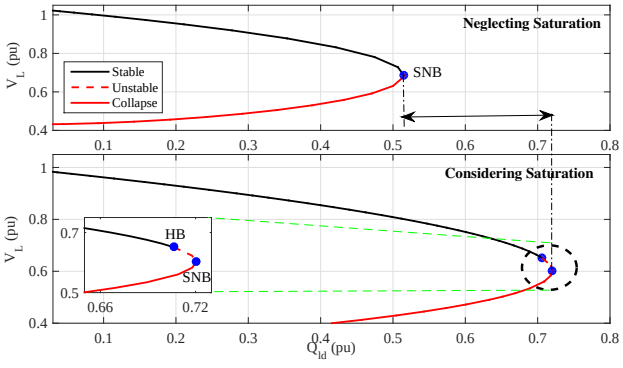

Fig. 6. Bifurcation analysis w.r.t. Q_{ld} (Top: Neglecting Saturation. Bottom: Considering Saturation)

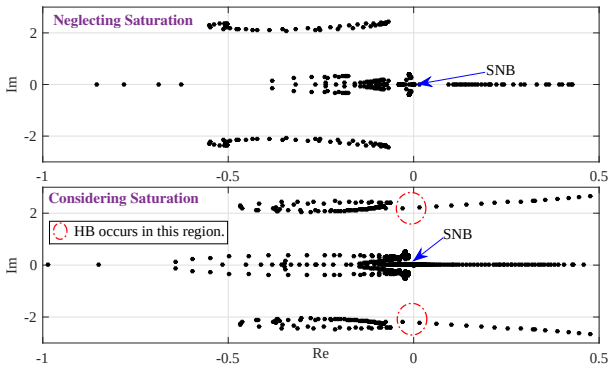

Fig. 7. Eigenvalues of the system after bifurcation analysis w.r.t. Q_{ld} (Top: Neglecting Saturation. Bottom: Considering Saturation)

when saturation is neglected, no Hopf bifurcation is detected in the system. However, detailed saturation modeling shows that one Hopf bifurcation exists in the system's dynamics. Further, results with detailed saturation modeling show $0.20554\ pu$ higher reactive loadability for the system before the SNB. Hence, in addition to the unrepresented bifurcation that exists in the nature of the system's dynamics, there is a significant difference in the reactive power loadability margin between the two cases. The eigenvalue loci for both cases are shown in Fig. 7.

IV. Bifurcation Analysis of the Multi-Machine Test System

To assess the applicability and scalability of the proposed method, bifurcation analysis is performed on the Western System Coordinating Council (WSCC) 9-bus multi-machine system. In this case, PSAT [20], a standard power systems analysis software, is modified and used for the purposes of bifurcation analysis, control design and its performance evaluation.

The bifurcation parameter of the system (λ) is considered to be the aggregated active load in all load buses of the system[1]. As mentioned in [18], the stationary branch of solutions should be derived, and bifurcation analysis has to be performed. This has been achieved by modifying and using the Continuation Power Flow (CPF) routine of PSAT. CPF allows to derive a continuum of power flow solutions w.r.t. the loading parameter, and helps in determining the voltage stability limit, i.e. SNB of the system. An important characteristic of the CPF is that it remains well-conditioned at and around the voltage stability limit. Consequently, divergence due to ill-conditioning is largely avoided at the SNB [21], [22]. PSATs source code has been modified to detect Hopf bifurcations after each CPF iteration. Bifurcation analysis results are shown in Table V. Note that the initial loading displayed was chosen and plotted very close to the HBs for the sake of clarity of the figure. As it is shown in Fig. 8, the system exhibits two Hopf bifurcations before reaching the saddle-node bifurcation. The bifurcation diagram of the system w.r.t. the voltage amplitude in bus 5 is

[1]In this case, the bifurcation parameter is considered to be the standard loading parameter of the system as it is in PSAT.

TABLE V
Bifurcations of the Multi-Machine Test System w.r.t. Loading Parameter λ

Point Type	EP	HB_1	HB_2	SNB
λ	0	0.0196	0.0586	1.0182

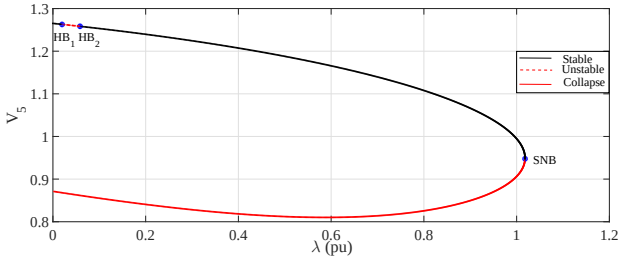

Fig. 8. Bifurcation analysis in the uncontrolled multi-machine test system w.r.t. λ

shown in Fig. 8. As it is depicted, the system undergoes Hopf bifurcations at $\lambda = 0.0196$ and $\lambda = 0.0586$. Also, the system collapses at $\lambda = 1.0182$. The eigenvalue loci of the system are depicted in Fig. 9, showing the two eigenvalue crossings of the imaginary axis related to the Hopf bifurcations.

V. Hopf Bifurcation Control

In this section, a dynamic state feedback controller is designed for relocating Hopf bifurcations using the results from Sections III and IV.

In the analyzed systems, one controller with a single input is sufficient to eliminate the Hopf bifurcations analyzed in Section III. For the single-machine test system, the *d*-axis stator current is chosen as the state used for the design of the state feedback control law; while for the multi-machine test system, the internal angle of synchronous generator number one is used. Hence, one single-input single-output control is added to each system in both cases.

A. Conditions of the Feasible Equilibria for Hopf Bifurcation Relocation

This section summarizes the steps of the algorithm used to select the equilibria to which the bifurcations can be (theoretically) relocated. The algorithm is formally described in detail in [18].

The dynamic state feedback controller relocates the existing Hopf bifurcations of the system to equilibria located after

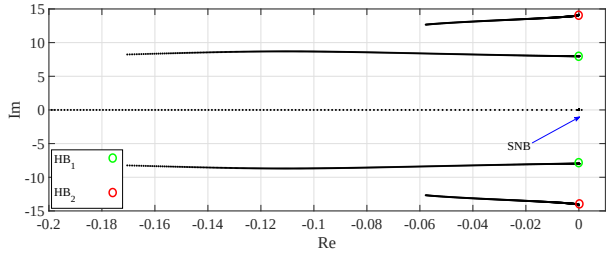

Fig. 9. Eigenvalues of the multi-machine test system after bifurcation analysis w.r.t. λ

TABLE VI
BIFURCATION ANALYSIS RESULTS IN THE CONTROLLED SINGLE-MACHINE TEST SYSTEM W.R.T. ACTIVE LOAD POWER

Point Type	EP	SNB	HB'_1	HB'_2
P_{ld}	0	1.024110	0.963149	0.798569

the occurrence of the SNB. The relocation process alters the stability status of the power system at its stationary equilibria. Because it cannot be guaranteed that all equilibria located after SNB are feasible from the stability point of view, a set of feasible equilibria are selected when they satisfy the following properties:

- The equilibria are located after the SNB.
- When relocating the Hopf bifurcations to this equilibria using the dynamic state feedback controller, the stability characteristics of the initial stable equilibrium point should not be altered.

B. Hopf Bifurcation Control w.r.t. P_{ld} in The Single-Machine Test System

According to the bifurcation analysis w.r.t. P_{ld}, the system undergoes two supercritical Hopf bifurcations. Although the bifurcations are supercritical and the associated limit cycles are stable, it is desirable to eliminate any oscillatory behavior from the system's responses. Hence, the introduced controller in Section V of [18] is employed. It should be noted that, because system experiences two Hopf bifurcations, two control gain vectors (K_1 and K_2) are required.

The equilibria of the uncontrolled system to which the bifurcations should be relocated are[1]

$$\begin{aligned} \bar{x}_1^{e1} &= [1.1, 1.93, 0, 0.54, 0, 1, -0.07, 0.61, -0.87]^T, \\ \bar{x}_2^{e2} &= [1.27, 1.93, 0, 0.50, 0, 1, 0.31, 0.51, -0.75]^T. \end{aligned} \tag{1}$$

These equilibria are located after the SNB, and the bifurcations occurring at these equilibria do not affect the stability of the system. For controller design, $l_1 = 0.1$ is used. Following the procedure introduced in Subsection V-C of [18], k_{11} is calculated at the first Hopf bifurcation point, and then k_{21} is calculated using the second Hopf bifurcation point. The control gains calculated to relocate the Hopf bifurcations are

$$\begin{aligned} k_{11} &= -0.1159, \\ k_{21} &= 0.00106. \end{aligned} \tag{2}$$

and the input and controller state equation are

$$\begin{aligned} u_1(x, y_{c_1}) &= -0.1159 i_d + 0.00106(i_d - 1.1)^2 - 0.1 y_{c_1}, \\ \dot{y_{c_1}} &= -0.1159 i_d + 0.00106(i_d - 1.1)^2 - 0.1 y_{c_1}. \end{aligned} \tag{3}$$

Next, bifurcation analysis is performed on the controlled system. Table VI presents the results. As it is observed, the Hopf bifurcations are successfully relocated to new positions and system is stable before reaching the SNB. The corresponding bifurcation diagram is presented in Fig. 10. In addition, the eigenvalue loci for the stationary branch of solutions of the controlled system are depicted in Fig.11. According to Fig. 11, eigenvalues are located in left side of the plane and system is stable before the SNB.

[1]Based on algorithm introduced in Section V-A.

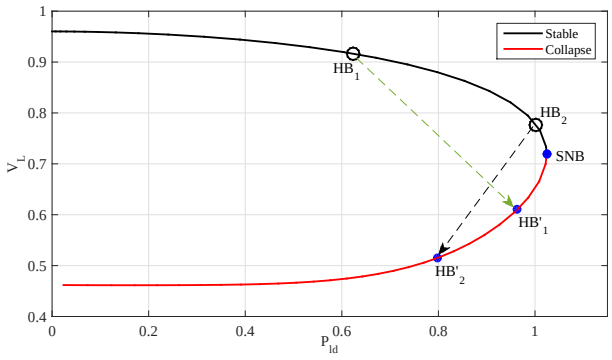

Fig. 10. Bifurcation analysis in the controlled single-machine test system w.r.t. P_{ld}

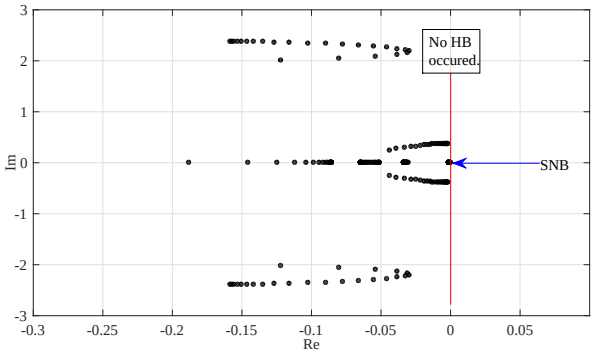

Fig. 11. Eigenvalues of the controlled single-machine test system after bifurcation analysis w.r.t. P_{ld}

C. Hopf Bifurcation Control w.r.t. Q_{ld} in The Single-Machine Test System

According to the bifurcation analysis w.r.t. reactive power load when saturation is modeled, the system undergoes one subcritical Hopf bifurcation. Hence, aside from the undesired oscillatory behavior, the resulting limit cycles are unstable and should be eliminated from system's response. The controller in Section V of [18] is designed. It should be noted that, because the system experiences only one Hopf bifurcation, only K_1 is required to relocate the subcritical Hopf bifurcation from the stable stationary branch of solutions. The equilibrium of the uncontrolled system to which the bifurcation should be relocated is

$$\bar{x}_1^{e1} = [0.87, 2.32, 0, 1.61, 0, 1, 0.38, 0.41, 0.34]^T. \tag{4}$$

The aforementioned equilibrium is located after the SNB, and a Hopf bifurcation occurring at this equilibrium does not affect the stability of the system. Only one control input is sufficient to relocate the Hopf bifurcation observed in III-B, and $l_1 = 0.001$ is used for controller design. Using the procedure from V-C of [18], k_{11} is calculated as

$$k_{11} = -0.001722845, \tag{5}$$

and the input and controller state equation are

$$\begin{aligned} u_1(x, y_{c_1}) &= -0.001722845 i_d - 0.001 y_{c_1}, \\ \dot{y_{c_1}} &= -0.001722845 i_d - 0.001 y_{c_1}. \end{aligned} \tag{6}$$

TABLE VII
BIFURCATION ANALYSIS RESULTS IN THE CONTROLLED SINGLE-MACHINE TEST SYSTEM W.R.T. REACTIVE LOAD POWER

Point Type	EP	SNB	HB
P_{ld}	0	0.720344	0.423637

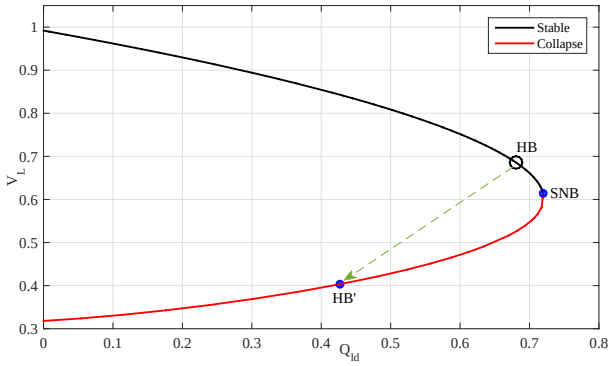

Fig. 12. Bifurcation analysis in the controlled single-machine test system w.r.t. Q_{ld}

Next,the bifurcation analysis is performed on the controlled system. Results are presented in Table VII. As it is observed, the Hopf bifurcation is successfully relocated to the new specified position and the system is stable before reaching the the SNB. The corresponding bifurcation diagram is presented in Fig. 12. In addition, the eigenvalue locus for the stationary branch of solutions for the controlled system is shown in Fig.13. As depicted in Fig. 13, the eigenvalues of the controlled system are located in the left side of the S-plane, before reaching the maximum reactive power loadability of the system. Hence, the system is stable on its stationary branch of solutions, and the risk of voltage collapse is eliminated. Because there are no stable operating points after the SNB where the HBs are relocated, the control objective is achieved successfully.

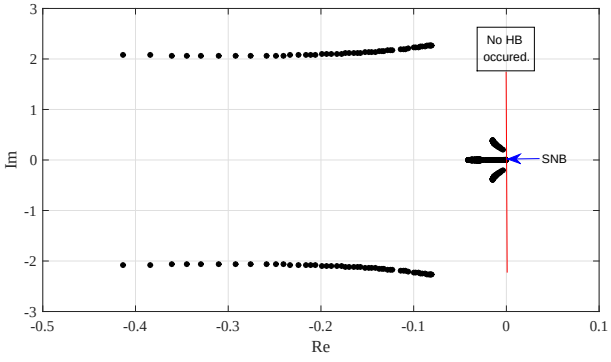

Fig. 13. Eigenvalues of the controlled single-machine test system after bifurcation analysis w.r.t. Q_{ld}

TABLE VIII
BIFURCATION ANALYSIS RESULTS IN THE CONTROLLED MULTI-MACHINE TEST SYSTEM W.R.T. λ

Point Type	EP	SNB	HB'_1	HB'_2
λ	0	1.0181	0.9072	0.9412

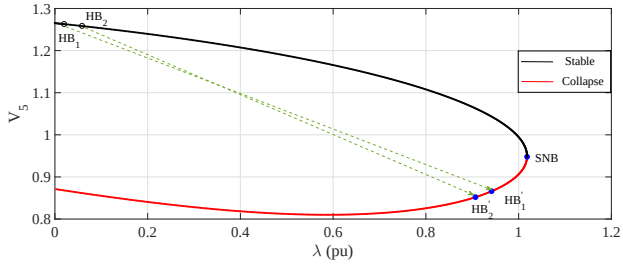

Fig. 14. Bifurcation analysis in the controlled multi-machine test system w.r.t. λ

D. Hopf Bifurcation Control in The Multi-Machine Test System

Using the results of Section IV, the objective is to relocate the two Hopf bifurcations. Hence, the controller in Section V-C of [18] is designed next. In this case, control gain vectors K_1 and K_2 are required to eliminate Hopf bifurcations from the solutions of the stable stationary branch. The equilibria of the uncontrolled system to which the bifurcations should be relocated are

$$\begin{aligned} \bar{x}_1^{e1} &= [0.03, 1, -4.51, 1, 0.30, 0.26, 1]^T \\ \bar{x}_2^{e2} &= [0.04, 1, -4.61, 1, 0.35, 0.27, 1]^T . \end{aligned} \tag{7}$$

These equilibria are located after the SNB, that is, in the stationary branch of solutions that are non-physically feasible operating points. In practice, this means that the HBs are removed from the space of feasible operating conditions of the grid.

For controller design, consider $l_1 = 0.5$. First, k_{11} is calculated at the first Hopf bifurcation point, and then k_{21} is calculated using the second Hopf bifurcation point. The control gains calculated for the relocation of Hopf bifurcations are

$$\begin{aligned} k_{11} &= -0.0091, \\ k_{21} &= 7.4093, \end{aligned} \tag{8}$$

and thus the control input and the controller state equation are:

$$\begin{aligned} u_1(x, y_{c_1}) &= -0.0091\delta_1 + 7.4093(\delta_1 - 0.03)^2 - 0.5y_{c_1}, \\ \dot{y_{c_1}} &= -0.0091\delta_1 + 7.4093(\delta_1 - 0.03)^2 - 0.5y_{c_1}. \end{aligned} \tag{9}$$

Next, bifurcation analysis is performed on the controlled system. Table VIII presents the results. As it is observed, Hopf bifurcations are successfully relocated to new positions and system is stable before reaching the SNB. The corresponding bifurcation diagram is presented in Fig. 14. In addition, the eigenvalue loci for the stationary branch of solutions of the controlled system are depicted in Fig.15. According to Fig. 15, the eigenvalues are located in left side of the plane and the system is stable before the SNB.

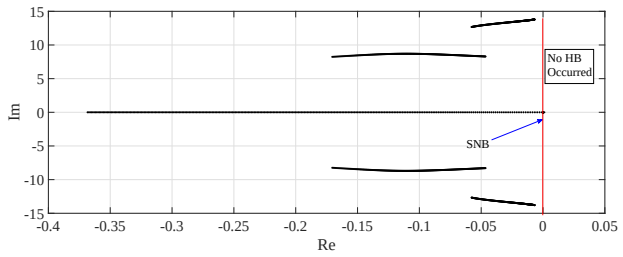

Fig. 15. Eigenvalues of the controlled multi-machine test system after bifurcation analysis w.r.t. λ

VI. Conclusion

This paper illustrated and demonstrated the applicability and scalability of the control design method proposed in Part I of this two-part paper [18]. The control design and its performance evaluation studies presented in this part allow drawing the following conclusions:

1) If saturation is not modeled in detail, the results of this paper show that:
   - Hopf bifurcations are not represented adequately.
   - Loadibility margins w.r.t. active and reactive powers are under-estimated.
2) For controller design, the feasible equilibria for relocation of Hopf bifurcations are required. To this end, this paper shows how the proposed algorithm detects feasible equilibria. In this algorithm, the equilibria after the saddle-node bifurcation (SNB) are selected as potential points to which Hopf bifurcations can be relocated. Next, the stability of the initial equilibrium point of the controlled system is assessed. If the initial operating point of the system is stable when relocating the Hopf bifurcations to selected equilibria, then they are considered as feasible equilibria for the controller.
3) When control gain vectors are obtained according to feasible equilibria for Hopf bifurcations relocation, the controller effectively relocates the Hopf bifurcations to their expected locations. Thus, this paper confirms the claims in Part I [18], providing a new control analysis and design method to mitigate voltage collapse caused by Hopf bifurcations.
4) In order to show the applicability and scalability of the proposed control design method in generic multi-machine power systems, the WSCC 9-bus system has been chosen for analysis. The results from a control design case study using this system show that after the addition of the controller designed for this system, two Hopf bifurcations are successfully relocated to the desired equilibria (located after the SNB), and stability of the system is preserved before reaching the maximum loadability margin.

In summary, in this paper (Part II) the effectiveness of the proposed dynamic state feedback control analysis and design method (proposed in Part I [18]) is validated via various analyses using multi-machine and single-machine power system models. The results help to illustrate, and to prove the applicability and scalability of the proposed control design method in generic power systems.

Acknowledgment

The authors would like to acknowledge the valuable inputs, fruitful comments, and discussions of Prof. Konstantin Turitsyn from Massachusetts Institute of Technology to this article. The quality of this work is substantially improved by his comments.

Appendix
System Parameters

In this appendix, system parameters are provided. All of the parameters are in per-unit. These parameters were obtained from [6], [23]. In addition, the parameters of the WSCC 9-bus system are taken from [24].

TABLE IX
Load Data

p_1	p_2	p_3	P_0	q_1	q_2	q_3	Q_0
0.24	1.7	0.2	0.4	-0.02	-1.866	1.4	0.8

TABLE X
Network Parameters

Y_1	Y_2	Y_3	ϕ_1	ϕ_2	ϕ_3
4.9752	1.6584	1.1056	-1.4711	-1.4711	-1.4711

TABLE XI
Synchronous Generator Parameters

R_s	Armature Winding Resistance	0.0043
R_f	Field Winding Resistance	0.0008
R_D	Damper Winding Resistance (d-axis)	0.0083
R_Q	Damper Winding Resistance (q-axis)	0.0190
L_{ls}	Armature Leakage Inductance	0.1360
L_{lf}	Field Winding Leakage Inductance	0.1833
L_{lD}	Damper Winding Leakage Inductance (d-axis)	0.1089
L_{lQ}	Damper Winding Leakage Inductance (q-axis)	0.1280
L_{md}	Direct Magnetizing Mutual Inductance (Unsaturated)	1.0125
L_{mq}	Quadrature Magnetizing Mutual Inductance (Unsaturated)	0.5840
H	Intertia Constant	1068.1
a	Turns Ratio	12.75

TABLE XII
Polynomial Coefficient a_{jk}

j \ k	0	1	2
0	1.581	-0.5986	-1.387
1	-0.5394	1.297	2.365
2	0.05049	-0.6299	-1.032

TABLE XIII
Polynomial Coefficient b_{jk}

j \ k	0	1	2	3
0	-0.4544	6.496	-8.642	3.173
1	-0.3300	14.46	-25.19	10.68
2	4.610	13.63	-36.88	17.60
3	0.3781	18.18	-34.21	14.94

REFERENCES

[1] I. Dobson and H.-D. Chiang, "Towards a theory of voltage collapse in electric power systems," *Systems & Control Letters*, vol. 13, no. 3, pp. 253–262, 1989.

[2] C.-W. Tan, M. Varghese, P. Varaiya, and F. Wu, "Bifurcation and chaos in power systems," *Sadhana*, vol. 18, no. 5, pp. 761–786, 1993.

[3] H.-D. Chiang, C.-W. Liu, P. Varaiya, F. Wu, and M. Lauby, "Chaos in a simple power system," *IEEE Trans. Power Syst.*, vol. 8, no. 4, pp. 1407–1417, 1993.

[4] E. H. Abed, H. Wang, J. Alexander, A. Hamdan, and H.-C. Lee, "Dynamic bifurcations in a power system model exhibiting voltage collapse," *Int'l J. of Bifurcation and Chaos*, vol. 3, no. 05, pp. 1169–1176, 1993.

[5] H.-D. Chiang, T. P. Conneen, and A. J. Flueck, "Bifurcations and chaos in electric power systems: Numerical studies," *J. of the Franklin Institute*, vol. 331, no. 6, pp. 1001 – 1036, 1994.

[6] K. Rajesh and K. Padiyar, "Bifurcation analysis of a three node power system with detailed models," *Int'l J. of Electrical Power & Energy Systems*, vol. 21, no. 5, pp. 375–393, 1999.

[7] Z. Jing, D. Xu, Y. Chang, and L. Chen, "Bifurcations, chaos, and system collapse in a three node power system," *Int'l J. of Electrical Power & Energy Systems*, vol. 25, no. 6, pp. 443 – 461, 2003.

[8] H.-D. Chiang, I. Dobson, R. J. Thomas, J. S. Thorp, and L. Fekih-Ahmed, "On voltage collapse in electric power systems," *IEEE Trans. Power Syst.*, vol. 5, no. 2, pp. 601–611, 1990.

[9] C. A. Canizares, "On bifurcations, voltage collapse and load modeling," *IEEE Trans. Power Syst.*, vol. 10, no. 1, pp. 512–522, 1995.

[10] B. Liscouski and W. Elliot, "Final report on the august 14, 2003 blackout in the united states and canada: Causes and recommendations," *A report to US Department of Energy*, vol. 40, no. 4, 2004.

[11] K. G. Boroojeni, M. H. Amini, and S. Iyengar, "Smart grids: Security and privacy issues," 2016.

[12] K. N. Srivastava and S. Srivastava, "Elimination of dynamic bifurcation and chaos in power systems using FACTS devices," *IEEE Trans. on Circuits and Systems I: Fundamental Theory and Applications*, vol. 45, no. 1, pp. 72–78, 1998.

[13] I. Ginarsa, A. Soeprijanto, and M. Purnomo, "Controlling chaos and voltage collapse using an ANFIS-based composite controller-static VAR compensator in power systems," *Int'l J. of Electrical Power & Energy Systems*, vol. 46, pp. 79 – 88, 2013.

[14] M. S. Widyan, "Controlling chaos and bifurcations of SMIB power system experiencing SSR phenomenon using SSSC," *Int'l J. of Electrical Power & Energy Systems*, vol. 49, pp. 66–75, 2013.

[15] A. M. Harb and N. Abdel-Jabbar, "Controlling Hopf bifurcation and chaos in a small power system," *Chaos, Solitons & Fractals*, vol. 18, no. 5, pp. 1055–1063, 2003.

[16] H. O. Wang and E. H. Abed, "Bifurcation control of a chaotic system," *Automatica*, vol. 31, no. 9, pp. 1213–1226, 1995.

[17] P. Yu and G. Chen, "Hopf bifurcation control using nonlinear feedback with polynomial functions," *Int'l J. of Bifurcation and Chaos*, vol. 14, no. 05, pp. 1683–1704, 2004.

[18] P. M. Vahdati, A. Kazemi, M. H. Amini, and L. Vanfretti, "Hopf bifurcation control in power systems nonlinear dynamics via dynamic state feedback controller—part I: Theory and modelling," *Accepted for publication in IEEE Trans. Power Systems.*, 2016, DOI:10.1109/TPWRS.2016.2633389.

[19] A. Dhooge, W. Govaerts, and Y. A. Kuznetsov, "Matcont: a MATLAB package for numerical bifurcation analysis of ODEs," *ACM Transactions on Mathematical Software (TOMS)*, vol. 29, no. 2, pp. 141–164, 2003.

[20] F. Milano, "An open source power system analysis toolbox," *IEEE Trans. Power Syst.*, vol. 20, no. 3, pp. 1199–1206, 2005.

[21] V. Ajjarapu and C. Christy, "The continuation power flow: a tool for steady state voltage stability analysis," *IEEE Trans. Power Syst.*, vol. 7, no. 1, pp. 416–423, 1992.

[22] A. J. Flueck and J. R. Dondeti, "A new continuation power flow tool for investigating the nonlinear effects of transmission branch parameter variations," *IEEE Trans. Power Syst.*, vol. 15, no. 1, pp. 223–227, 2000.

[23] M. Despalatović, M. Jadrić, and B. Terzić, "Modeling of saturated synchronous generator based on steady-state operating data," *IEEE Trans. on Industry Applications*, vol. 48, no. 1, pp. 62–69, 2012.

[24] P. M. Anderson and A. A. Fouad, *Power system control and stability*. John Wiley & Sons, 2008.

Pouya Mahdavipour Vahdati (S'16) is currently pursuing the Ph.D. in Mechatronic Systems at KTH Royal Institute of Technology, Stockholm, Sweden. In 2015, he received the M.Sc. degree in Electrical Engineering from Center of Excellence for Power Systems Automation and Operation, Iran University of Science and Technology, Tehran, Iran. He is a member of Innovative Training Network for Optimization of Cyper-Physical Systems (oCPS), and he is the recipient of COST Action grant of DSM-TP in 2016. His research interests include power systems dynamics, control theory, bifurcation theory, and dynamics of cyber-physical systems.

Luigi Vanfretti (SM'15) obtained the M.Sc. and Ph.D. degrees in electric power engineering at Rensselaer Polytechnic Institute, Troy, NY, USA, in 2007 and 2009, respectively. He is an Associate Professor (Tenured) and Docent at KTH Royal Institute of Technology, Stockholm, Sweden, where he has been a faculty member since 2010. His research interests are in the area of synchrophasor technology applications, and cyber-physical power system modeling, simulation, stability and control.

M. Hadi Amini (S'11) is currently pursuing the dual-degree Ph.D. in Electrical and Computer Engineering at Carnegie Mellon University (CMU), and SYSU-CMU Joint Institute of Engineering. Prior to that, he received the M.Sc. degrees in Electrical and Computer Engineering from Carnegie Mellon University in 2015, and Tarbiat Modares University in 2013, and the B.Sc. degree in Electrical Engineering from Sharif University of Technology in 2011. He is the recipient of Sustainable Mobility Summer Fellowship from Massachusetts Institute of Technology (MIT) office of Sustainability in 2015, and the deans honorary award from the president of Sharif University of Technology in 2007. His research interests are power systems optimization, electric vehicles, and interdependent networks. (homepage: www.HadiAmini.com)

Ahad Kazemi received his M.Sc. degree in electrical engineering from Oklahoma State University, Stillwater, in 1979. Currently, he is an Associate Professor in the Electrical Engineering Department, Iran University of Science and Technology, Tehran, Iran. His research interests are reactive power control, power system dynamics, and stability and control and Flexible AC Transmission Systems devices.